

# The Search for Multiple Populations in Magellanic Cloud Clusters III: No evidence for Multiple Populations in the SMC cluster NGC 419

S. Martocchia<sup>1</sup>, N. Bastian<sup>1</sup>, C. Usher<sup>1</sup>, V. Kozhurina-Platais<sup>2</sup>, F. Niederhofer<sup>2,3</sup>, I. Cabrera-Ziri<sup>1</sup>, E. Dalessandro<sup>4</sup>, K. Hollyhead<sup>1</sup>, N. Kacharov<sup>5</sup>, C. Lardo<sup>1</sup>, S. Larsen<sup>6</sup>, A. Mucciarelli<sup>7</sup>, I. Platais<sup>8</sup>, M. Salaris<sup>1</sup>, M. Cordero<sup>9</sup>, D. Geisler<sup>10</sup>, M. Hilker<sup>11</sup>, C. Li<sup>12</sup>, D. Mackey<sup>13</sup>

<sup>1</sup>*Astrophysics Research Institute, Liverpool John Moores University, 146 Brownlow Hill, Liverpool L3 5RF, UK*

<sup>2</sup>*Space Telescope Science Institute, 3700 San Martin Drive, Baltimore, MD 21218, USA*

<sup>3</sup>*Leibniz-Institut für Astrophysik Potsdam, An der Sternwarte 16, Potsdam 14482, Germany*

<sup>4</sup>*INAF, Osservatorio Astronomico di Bologna, via Ranzani 1, 40127, Bologna, Italy*

<sup>5</sup>*Max-Planck-Institut für Astronomie, Königstuhl 17, D-69117 Heidelberg, Germany*

<sup>6</sup>*Department of Astrophysics/IMAPP, Radboud University, P.O. Box 9010, 6500 GL Nijmegen, The Netherlands*

<sup>7</sup>*Department of Physics and Astronomy, University of Bologna, Viale Berti Pichat 6/2, I-40127 Bologna, Italy*

<sup>8</sup>*Department of Physics and Astronomy, Johns Hopkins University, 3400 North Charles Street, Baltimore, MD 21218, USA*

<sup>9</sup>*Astronomisches Rechen-Institut, Zentrum für Astronomie der Universität Heidelberg, Mönchhofstrasse 12-14, D-69120 Heidelberg, Germany*

<sup>10</sup>*Departamento de Astronomia, Universidad de Concepcion, Casilla 160-C, Chile*

<sup>11</sup>*European Southern Observatory, Karl-Schwarzschild-Straße 2, D-85748 Garching bei München, Germany*

<sup>12</sup>*Department of Physics and Astronomy, Macquarie University, Sydney, NSW 2109, Australia*

<sup>13</sup>*Research School of Astronomy and Astrophysics, Australian National University, Canberra, ACT 2611, Australia*

Accepted. Received ; in original form.

## ABSTRACT

We present the third paper about our ongoing HST survey for the search for multiple stellar populations (MPs) within Magellanic Cloud clusters. We report here the analysis of NGC 419, a  $\sim 1.5$  Gyr old, massive ( $\gtrsim 2 \times 10^5 M_{\odot}$ ) star cluster in the Small Magellanic Cloud (SMC). By comparing our photometric data with stellar isochrones, we set a limit on [N/Fe] enhancement of  $\lesssim +0.5$  dex and hence we find that no MPs are detected in this cluster. This is surprising because, in the first two papers of this series, we found evidence for MPs in 4 other SMC clusters (NGC 121; Lindsay 1, NGC 339, NGC 416), aged from 6 Gyr up to  $\sim 10 - 11$  Gyr. This finding raises the question whether age could play a major role in the MPs phenomenon. Additionally, our results appear to exclude mass or environment as the only key factors regulating the existence of a chemical enrichment, since all clusters studied so far in this survey are equally massive ( $\sim 1 - 2 \times 10^5 M_{\odot}$ ) and no particular patterns are found when looking at their spatial distribution in the SMC.

**Key words:** galaxies: star clusters: individual: NGC 419 – galaxies: individual: SMC – Hertzsprung-Russell and colour-magnitude diagrams – stars: abundances

## 1 INTRODUCTION

In the last few decades, our understanding of globular clusters (GCs) as simple stellar populations (SSPs) has been overturned by the presence of star-to-star abundance spreads in light elements (e.g., C, N, O, Na) and by the broadening/splitting of features in clusters' colour-magnitude diagrams (CMDs).

The presence of multiple stellar populations (MPs) in

GCs appears to be nearly ubiquitous in the most nearby galaxies. Large numbers of Milky Way GCs have been studied (Gratton, Carretta & Bragaglia 2012) and all old ( $> 10$  Gyr) clusters surveyed so far have been found to host MPs (with the single exception being Ruprecht 106, Vilanova et al. 2013). This is also found in the Fornax dwarf galaxy (Larsen et al. 2014b), the Sagittarius dwarf galaxy (Carretta et al. 2014), the WLM dwarf galaxy (Larsen et al. 2014a) and in the Large Magellanic Cloud (LMC,

Mucciarelli et al. 2009). Recently, MPs were also detected in the  $\sim 10$  Gyr-old Small Magellanic Cloud (SMC) cluster NGC 121 (Dalessandro et al. 2016 and Niederhofer et al. 2017b, Paper I hereafter).

Indeed, until recently, MPs were believed to be found only in massive, old clusters, while none were present in clusters of comparable age and lower masses (e.g., E3, Salinas & Strader 2015). Such evidence led many to consider mass as the key cluster property controlling the presence of MPs (e.g., Gratton, Carretta & Bragaglia 2012). The discovery of relatively young ( $\sim 1 - 2$  Gyr old), but still massive ( $\lesssim 2 \times 10^5 M_{\odot}$ ) clusters with no abundance spreads within them (Mucciarelli et al. 2008, 2014, Colucci et al. 2012) challenged this scenario. In addition to this, Mucciarelli et al. (2011) analysed the spectra of red giant branch (RGB) stars in NGC 1866, a very young ( $\sim 200$  Myr) and massive ( $\sim 1 \times 10^5 M_{\odot}$ ) cluster, finding no evidence for MPs. Although these results were based on a relatively small sample of stars with spectroscopically determined abundances, such findings have opened a new question about whether age could be considered as a relevant factor for the existence of MPs, as well as mass. The goal of our ongoing HST survey is to provide new insights into this phenomenon.

Hollyhead et al. (2017) spectroscopically detected MPs in the SMC cluster Lindsay 1 which is massive ( $\sim 10^5 M_{\odot}$ ) and relatively young ( $\sim 8$  Gyr old). Niederhofer et al. (2017a) (Paper II hereafter) photometrically confirmed the result by Hollyhead et al. (2017) for Lindsay 1 and showed that MPs are present in two other intermediate-age SMC clusters, namely NGC 339 and NGC 416, similar in mass and age to Lindsay 1. Also, Hollyhead et al. (in prep.) have detected MPs in Kron 3, another SMC cluster which is  $\sim 6.5$  Gyr old and as massive as  $\sim 2 \times 10^5 M_{\odot}$ . All these massive clusters fall in a range of ages (i.e., 6 – 8 Gyr) which have never been explored. So far, Lindsay 1, NGC 339, NGC 416 and Kron 3 represent the youngest clusters that have been found to host MPs. This surprising result suggests that the MPs phenomenon is not a cosmological effect, as it operated at least down to  $z = 0.65$ , well past the peak epoch of GC formation ( $z \gtrsim 2$ , e.g. Brodie & Strader 2006).

Here we present the analysis of NGC 419, a young ( $\sim 1.5$  Gyr, Glatt et al. 2008), massive ( $\gtrsim 2 \times 10^5 M_{\odot}$ , Goudfrooij et al. 2014) SMC cluster, one of the targets of our photometric survey of Magellanic Clouds (MCs) star clusters (Paper I & II). So far in our survey, we detected MPs in the SMC clusters NGC 121 (Paper I), NGC 339, NGC 416 and Lindsay 1 (Paper II). Here we will show that there is no evidence for multiple sequences/broadening in the RGB of NGC 419.

NGC 419 shows one of the most extended main sequence turnoffs (eMSTOs) in clusters analysed so far, a common peculiarity of intermediate and young age MC massive clusters, from 1 – 2 Gyr (e.g. Mackey et al. 2008, Milone et al. 2009) down to  $\sim 100$  Myr (Bastian et al. 2016). Originally, an eMSTO was thought to be caused by age spreads of  $\sim 200 - 700$  Myr (e.g. Goudfrooij et al. 2014) due to multiple star formation (SF) events. According to this hypothesis, NGC 419 should have a very large age spread,  $\sim 700$  Myr (Rubele, Kerber & Girardi 2010). However, subsequent works have shown that such features seem more likely due to a single age population with a range of stellar rotation rates

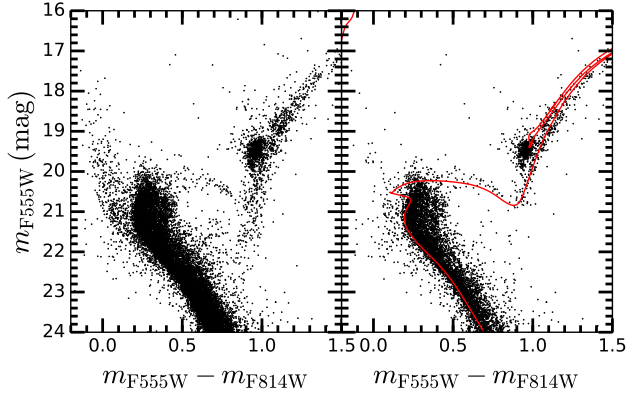


**Figure 1.**  $m_{F555W} - m_{F814W}$  vs.  $m_{F555W}$  CMD of NGC 419 before (left) and after (right) the field star subtraction. The red curve in the right panel indicates the MIST isochrone we adopted for values of age (1.4 Gyr) and metallicity ( $[Fe/H] = -0.7$ ).

(Bastian & de Mink 2009, Niederhofer et al. 2015, Brandt & Huang 2015).

This paper is organised as follows: in §2.1 and §2.2 we describe the observation of NGC 419 and data reduction procedures, while in §2.3 we report the analysis of the cluster. In §3 we give an outline about the stellar evolution models we used and in §4 we present our results of comparison between data and models. Finally, we discuss our results and conclusions in §5.

## 2 OBSERVATIONS AND DATA REDUCTION

### 2.1 Data and Photometry

Photometric data for NGC 419 were obtained from the ongoing *Hubble Space Telescope* survey GO-14069 (P.I. N. Bastian, see Paper I)<sup>1</sup>. New observations were provided for the optical wide band filter  $F438W$  and the UV narrow band filter  $F343N$  (WFC3/UVIS instrument). Archival data were used for the UV band filter  $F336W$  (WFC3/UVIS, GO-12257, P.I. L. Girardi), and for the optical bands  $F555W$  and  $F814W$  (ACS/WFC, GO-10396, P.I. J. Gallagher).

The UV/optical filters are extremely useful when searching for MPs. Strong NH absorption lines are present inside the  $F336W$  and  $F343N$  filter bands, while the  $F438W$  passband includes CH absorption features (Piotto et al. 2015 and Fig. 1 in Paper I). Both  $F555W$  and  $F814W$  filters were used to select RGB stars, while the  $F814W$  one, along with  $F343N$ ,  $F336W$ ,  $F438W$ , was also used to compose a suitable colour combination for revealing the presence of MPs (see §2.3).

Both ACS/WFC and WFC3/UVIS observations were processed through the standard HST pipeline. The photometry for NGC 419 was determined by applying the point spread function (PSF) fitting method, using the spatial variable “effective PSF” (ePSF) libraries (Anderson & King 2006). We refer to Paper I and Paper II for more specific details about data processing and photometry.

<sup>1</sup> The photometric catalogues are available from the authors upon request.

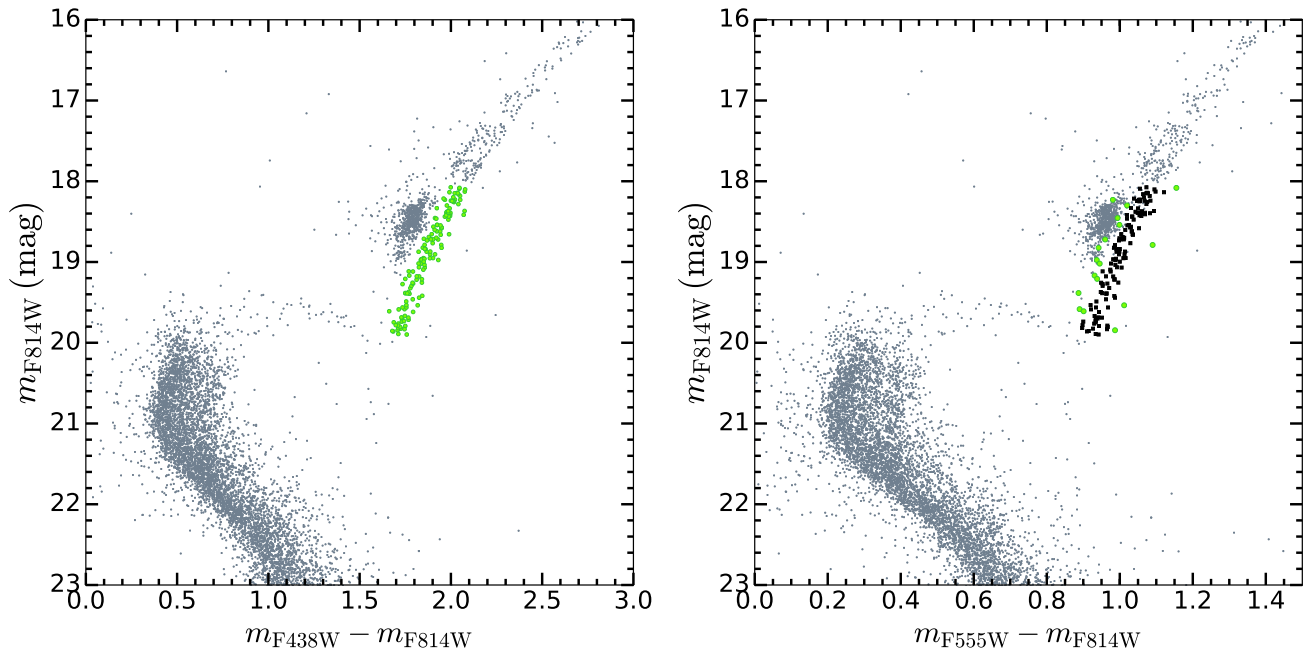


**Figure 2.** *Left panel:* CMD of NGC 419 using  $m_{F438W} - m_{F814W}$  vs.  $m_{F814W}$ . Green filled circles mark the RGB stars selected in this colour and magnitude combination. *Right Panel:*  $m_{F555W} - m_{F814W}$  vs.  $m_{F814W}$  CMD of NGC 419. Black filled squares indicate the second selection of RGB stars in this colour-magnitude space, while green filled circles represent the stars passing the initial selection but not the second.

To select cluster members, we considered stars that are within 900 pixels from the center of NGC 419, which corresponds to  $36''$  ( $0.04''$  pixel scale for the WFC3/UVIS instrument). We then defined a background reference region with the same area as the cluster region in order to statistically subtract field stars from the cluster CMD in  $m_{F336W} - m_{F438W}$  vs.  $m_{F438W}$  space. For every star in the background region, the closest star in colour-magnitude space in the cluster region is removed. Fig. 1 shows the  $m_{F555W} - m_{F814W}$  vs.  $m_{F555W}$  CMD of NGC 419, before (left panel) and after (right panel) the field star subtraction.

## 2.2 Differential Reddening

We also investigated possible effects of differential reddening on our CMDs, even if the level of extinction towards NGC 419 is quite low ( $A_V \simeq 0.15$ , Goudfrooij et al. 2014). We corrected the photometry of NGC 419 for differential reddening following the method described in Milone et al. (2012) and using the extinction coefficients reported in Milone et al. (2015). The average change in colour due to differential extinction in both  $m_{F336W} - m_{F438W}$  and  $m_{F343N} - m_{F438W}$  colours results to be  $< 0.01$ , with a maximum  $A_{F336W} = 0.02$ . We conclude that reddening effects are negligible and do not affect our results. Thus, we did not account for the differential extinction correction in our analysis.

## 2.3 Analysis

In order to search for the presence of multiple populations, we need to select a clean sample of RGB cluster members. To be as conservative as possible, we selected RGB stars

in three different colour-magnitude spaces. This reduces the contamination by SMC field stars with ages  $\sim 1$  Gyr, comparable to the age of NGC 419. The first selection was made in  $F438W - F814W$  colours. Indeed, these colours are the best at separating the RGB from the Asymptotic Giant Branch (AGB) and the Horizontal Branch (HB). Optical colours are much less affected by sensitive star-to-star N variations than other colour combinations with a passband encompassing the NH and CN molecular features, i.e. the F336W and F343N filters (Sbordone et al. 2011). The left panel of Figure 2 shows the  $m_{F438W} - m_{F814W}$  vs.  $m_{F814W}$  CMD of NGC 419. Green filled circles mark the RGB stars selected in this filter combination. To avoid contamination by AGB stars, a brightness cut was applied ( $m_{F814W} > 18$ ). We then plotted these RGB stars on the  $m_{F555W} - m_{F814W}$  vs.  $m_{F814W}$  CMD of NGC 419. We noticed that several objects were scattered off the RGB or found to belong to the red clump, hence we made a second selection in  $F555W - F814W$  colours. The right panel of Fig. 2 shows the  $m_{F555W} - m_{F814W}$  vs.  $m_{F814W}$  CMD of NGC 419 with black filled squares indicating the second selection of RGB stars. Green filled circles mark the stars passing the first selection criterion but not the second. Also note that Fig. 2 shows NGC 419’s remarkable eMSTO.

We then plotted the second selection of RGB stars on the  $m_{F336W} - m_{F438W}$  vs.  $m_{F438W}$  CMD. Again, we found a very few objects which scattered off the RGB or on the tip of the MS (5 out of  $> 100$  stars). We made the final selection in  $F336W - F438W$  colours and this is shown in the left panel of Fig. 3, where the  $m_{F336W} - m_{F438W}$  vs.  $m_{F438W}$  CMD of NGC 419 is displayed. The right panel of Fig. 3 shows the CMD of NGC 419 using the narrow band filter F343N, in the  $m_{F343N} - m_{F438W}$  vs.  $m_{F438W}$  space. Red filled circles mark the final selected RGB stars in both panels of Fig. 3. Black

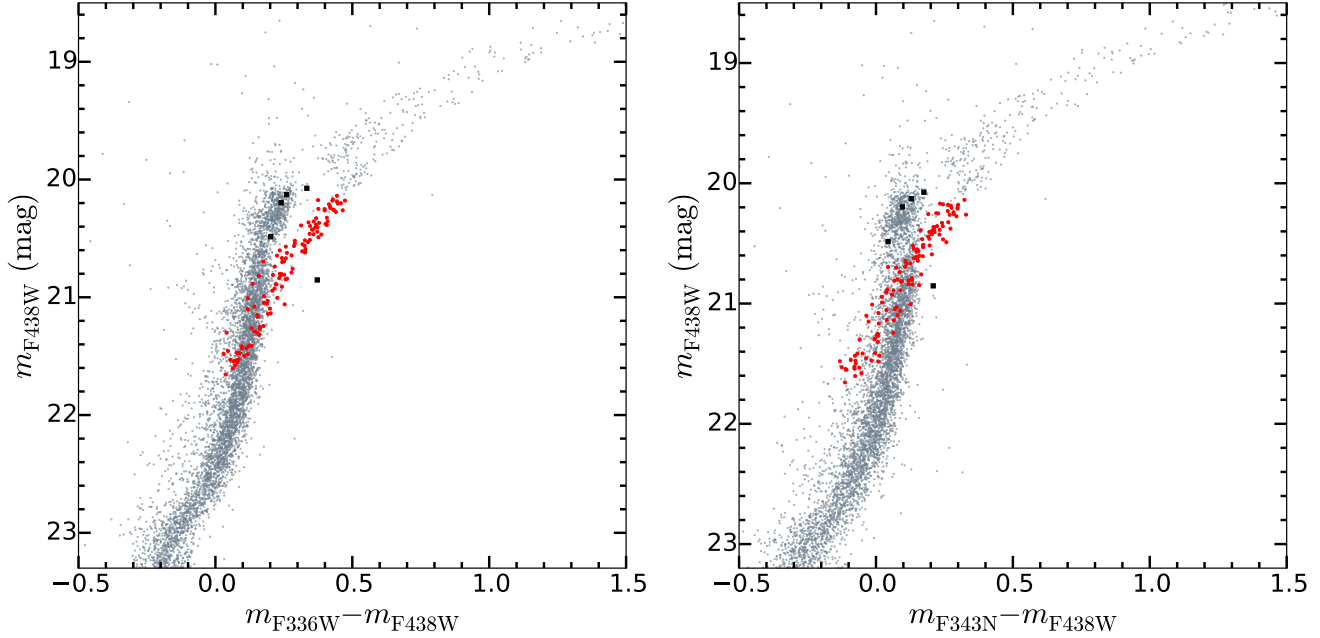


**Figure 3.**  $m_{F336W} - m_{F438W}$  vs.  $m_{F438W}$  CMD (left panel) and  $m_{F343N} - m_{F438W}$  vs.  $m_{F438W}$  CMD (right panel) of NGC 419. Red filled circles indicate the final RGB selected stars, while black filled squares represent the stars which did not pass the final selection.

filled squares represent the stars that did not pass the third selection. Interestingly, the RGB stars superimpose on the main sequence in these filters, emphasizing the importance of a selection in other colours such as  $F438W - F814W$  and  $F555W - F814W$ .

A first look at the  $m_{F336W} - m_{F438W}$  and  $m_{F343N} - m_{F438W}$  vs.  $m_{F438W}$  diagrams reveals that no splitting is detected in the RGB. The presence of multiple sequences and/or broadening in the RGB is a clear indication of the existence of two or more populations of stars, one with a primordial chemical composition, the others with a certain level of chemical enrichment (depleted in C and O and enhanced in N). Accordingly, we performed an analysis in order to quantify the observed spread in the UV/optical CMDs of NGC 419. More specifically, we analysed the differences between the spreads in the two filters,  $F336W$  and  $F343N$ .

We used a filter combination of the form  $(F336W - F438W) - (F438W - F814W) = C_{F336W, F438W, F814W}$  for the wide band F336W and  $(F343N - F438W) - (F438W - F814W) = C_{F343N, F438W, F814W}$  for the narrow band F343N. Monelli et al. (2013) used a similar filter combination in order to detect the presence of MPs in a number of Galactic GCs, the  $C_{U,B,I} = (U - B) - (B - I)$  combination. They point out that this pseudo-colour is effective at unveiling multiple sequences and spreads in the RGB (see also §3 and §4 for model predictions). Another advantage of this pseudo-colour at the age of NGC 419 is that the RGB is almost vertical. The same colour ( $C_{F336W, F438W, F814W}$ ) has also recently been used by Dalessandro et al. (2016) to efficiently detect MPs in NGC 121. The top panels of Figures 4 and 5 show the CMDs of NGC 419 using  $C_{F336W, F438W, F814W}$  vs.  $m_{F438W}$  and  $C_{F343N, F438W, F814W}$  vs.  $m_{F438W}$ , respectively. Orange and green circles indicate the selected RGB stars in the two different CMDs. No evidence of multiple sequences is seen in such filter combinations either. The bottom panels of

Figures 4 and 5 show the histograms of the distributions in  $C_{F336W, F438W, F814W}$  and  $C_{F343N, F438W, F814W}$  colours of the RGB stars in NGC 419, respectively. Hereafter, we will refer to  $C_{F336W, F438W, F814W}$  as CUBI and to  $C_{F343N, F438W, F814W}$  as CUnBI for more clarity, unless stated otherwise.

We calculated the mean and standard deviation ( $\sigma$ ) on unbinned colours (i.e., CUBI and CUnBI) and derived a Gaussian PDF, indicated as a grey curve in the bottom panels of Fig. 4 and 5. The obtained  $\sigma$  values are  $\simeq 0.04$  for both filter combinations, with a difference of only  $\sim 2 \times 10^{-4}$ . We calculated the statistical error on  $\sigma$ . Using a bootstrap technique based on 10000 realisations, we found that  $\sigma_{\text{CUBI}} = 0.043 \pm 0.004$  and  $\sigma_{\text{CUnBI}} = 0.043 \pm 0.003$ . As far as photometric errors are concerned, these are essentially the same in F336W and F343N filters in this bright regime. Therefore, we can say that errors are the same for both CUBI and CUnBI. Hence, the observed RGB widths in CUBI and CUnBI colours are directly comparable. In addition to this, the photometric errors in CUBI and CUnBI colours are comparable to the observed spreads.

We derived the kernel density distribution (KDE) from a Gaussian kernel for both CUBI and CUnBI colours. The results are superimposed on the histograms of data in the bottom panels of Fig. 4 and 5, as orange and green solid curves respectively. By visual inspection, we were unable to detect any significant difference between the gaussian and KDE distributions. The KDE did not reveal any bimodality or peaks that the gaussian could have smoothed out. Indeed, the dip test for unimodality (Hartigan & Hartigan 1985) confirms that there is no statistically significant bimodality in either the CUBI or CUnBI distribution.

We also provided a different estimate for the RGB width. We defined the  $W_{\text{RGB}}$  index as the colour extension of the KDE at 20% of the distribution maximum. The values of  $W_{\text{RGB}}$  for CUBI and CUnBI are given in the bot-

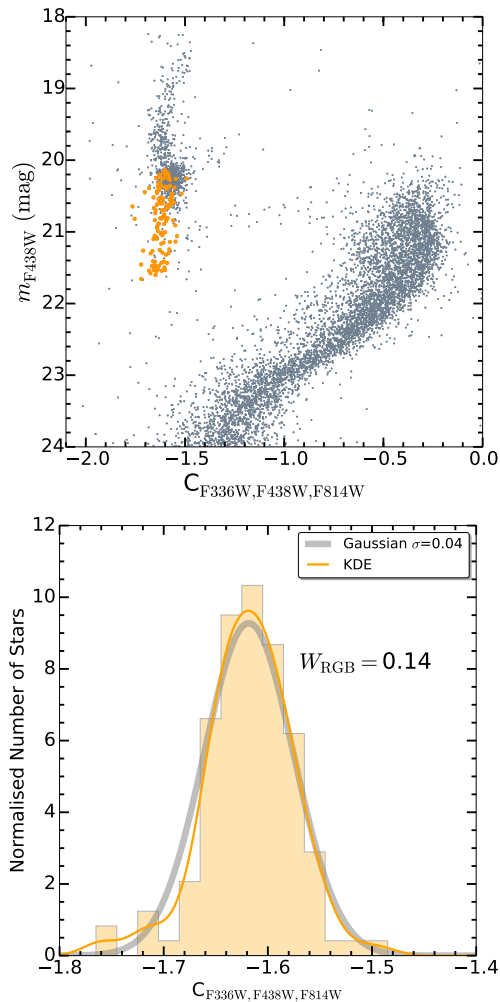


**Figure 4.** *Top Panel:*  $C_{F336W,F438W,F814W}$  vs.  $m_{F438W}$  CMD of NGC 419. Orange filled circles mark the selected RGB stars. *Bottom Panel:* histogram of the distribution of RGB stars in NGC 419, in  $C_{F336W,F438W,F814W}$  colours. The grey solid curve represents the Gaussian probability density function (PDF) with mean and standard deviation ( $\sigma$ ) calculated on unbinned data, while the orange solid curve indicates the KDE. Superimposed on the plot is the  $W_{\text{RGB}}$  index, see text for more details.

tom panels of Figs. 4 and 5, respectively. We estimated the error on the  $W_{\text{RGB}}$  index using a Monte Carlo simulator technique. We obtained  $W_{\text{RGB}} = 0.139 \pm 0.013$  for CUBI and  $W_{\text{RGB}} = 0.157 \pm 0.013$  for CUnBI. This confirms that the two widths are comparable, at  $\sim 1\sigma$  confidence level.

Synthetic spectra which take into account the presence of multiple population, i.e. the presence of enriched stars with respect to the primordial ones, predict a significant difference in the observed RGB spread when using the wide-band  $F336W$  filter with respect to the narrow-band  $F343N$  filter (see §3). More specifically, we observe that  $\sigma_{\text{CUnBI}} \simeq \sigma_{\text{CUBI}} \simeq 0.04$  but we would have expected  $\sigma_{\text{CUnBI}} \gtrsim 0.1$  if MPs were present (§4). If the spreads are caused only by photometric errors, then we would expect  $\sigma_{\text{CUBI}} \simeq \sigma_{\text{CUnBI}}$ , which is what we observe. No clear difference is detected in the observed spreads and  $W_{\text{RGB}}$  indices between CUBI and CUnBI colours, hence we do not detect multiple populations

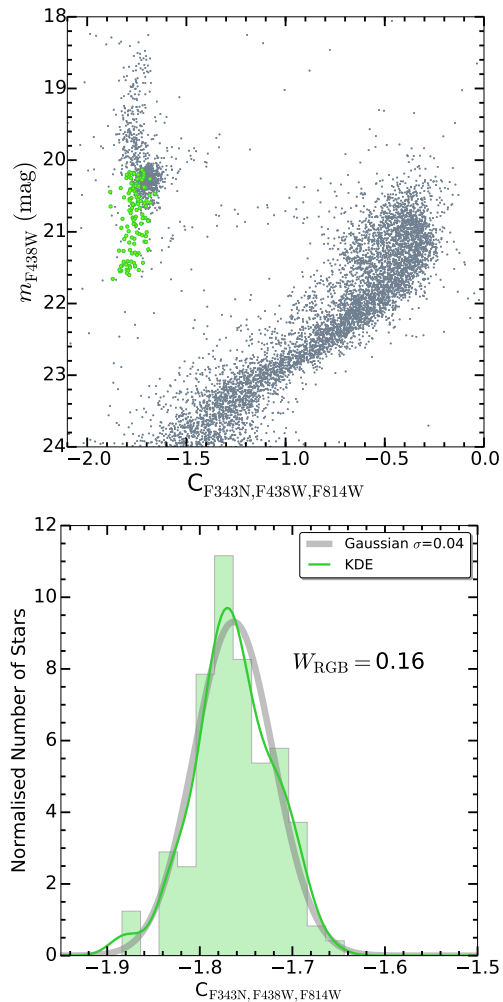


**Figure 5.** *Top Panel:*  $C_{F343N,F438W,F814W}$  vs.  $m_{F438W}$  CMD of NGC 419. Green filled circles mark the selected RGB stars. *Bottom Panel:* histogram of the distribution of RGB stars in NGC 419, in  $C_{F343N,F438W,F814W}$  colours. The grey solid curve represents the Gaussian probability density function (PDF) with mean and standard deviation ( $\sigma$ ) calculated on unbinned data, while the green solid curve indicates the KDE. Superimposed on the plot is the  $W_{\text{RGB}}$  index, see text for more details.

in the RGB of NGC 419. We will discuss in detail these outcomes in Section 4.

Finally, we also looked at observed spreads in the Red Clump (RC) and upper RGB (URGB). We performed the same analysis as for the RGB. We obtained that the widths are the same for CUBI and CUnBI in the RC ( $W_{\text{RC}} \simeq 0.12$ ). We observe a slightly larger spread for CUnBI with respect to CUBI in the URGB ( $W_{\text{URGB}}(\text{CUBI}) = 0.105 \pm 0.012$ ,  $W_{\text{URGB}}(\text{CUnBI}) = 0.129 \pm 0.016$ ), although these are comparable at  $\sim 1\sigma$  level when taking the error into account.

### 3 MODELS

In this Section, we report on how we calculated stellar evolution models with different levels of chemical enrichment, in order to compare them with our observations. We describe the estimation of age and metallicity in §3.1 and we out-

line the calculation of models in §3.2. In §3.3, we consider possible effects of an enhanced He abundance on the RGB.

### 3.1 Age, Extinction and Distance Modulus

We used MIST isochrones (Dotter 2016; Choi et al. 2016) for several ages ( $\log[t/\text{yr}] = 9.1, 9.15, 9.2, 9.25$ ) and metallicities ( $[\text{Fe}/\text{H}] = -0.6, -0.7, -0.75$ ). We then assumed the distance modulus  $M - m = 18.85$  and extinction value  $A_V = 0.15$  for NGC 419 from Goudfrooij et al. (2014), in order to match data to the isochrones. For the other filter extinction values, we used  $A_{F336W} = 1.64 A_V$ ,  $A_{F343N} = 1.64 A_V$ ,  $A_{F438W} = 1.35 A_V$ ,  $A_{F555W} = 1.055 A_V$ ,  $A_{F814W} = 0.586 A_V$  (Milone et al. 2015; Goudfrooij et al. 2009). We selected  $\log[t/\text{yr}] = 9.15$  ( $t \simeq 1.4$  Gyr) and  $[\text{Fe}/\text{H}] = -0.7$  as the parameters which best describe the observed  $m_{F555W} - m_{F814W}$  vs.  $m_{F814W}$  CMD of NGC 419 by eye. This is in agreement with the results by Goudfrooij et al. (2014). In addition to this, we also agree with Glatt et al. (2008), who perform several isochrones fitting, which yield values ranging from 1.2 to 1.6 Gyr. The selected isochrone is shown on the  $m_{F555W} - m_{F814W}$  vs.  $m_{F555W}$  CMD of NGC 419 in the right panel of Fig. 1 as a red curve.

### 3.2 Abundance Anomalies

We calculated synthetic photometry from model atmospheres with different abundance patterns. We used version 1.0 of the MIST isochrones (Choi et al. 2016) with an age of 1.41 Gyr and a metallicity of  $[\text{Fe}/\text{H}] = -0.70$  to provide input parameters for our model atmospheres (see §3.1). The 1-D MIST models include a range of physics including diffusion on the MS, rotation in stars more massive than  $1.2 M_\odot$ , convection including thermohaline and rotational mixing. We used ATLAS12 (Kurucz 1970, 2005) to calculate model atmospheres and SYNTHÉ (Kurucz & Furenlid 1979; Kurucz & Avrett 1981) to synthesize spectra. These models are one-dimensional, static and plane parallel and assume local thermodynamic equilibrium. We used the same versions of the models used by Sbordone et al. (2004) and line lists for the atomic data as Larsen, Brodie & Strader (2012) and Larsen et al. (2014b) who we refer to for further details of our stellar atmosphere calculations. We also utilise the same PYTHON wrappers to ATLAS12 and SYNTHÉ as used by Larsen, Brodie & Strader (2012). For our stellar atmosphere calculations we adopted the Asplund et al. (2009) solar abundances which are the same as adopted by the MIST models. For each set of models, we calculated 57 model spectra between  $0.7 M_\odot$  on the MS and the tip of the RGB. We selected the input masses to calculate model atmospheres by eye in  $\log L - \log T_{\text{eff}}$  space with denser sampling during stellar evolutionary phases such as the MSTO and the base of the RGB where the isochrone displays greater curvature.

We calculated the models using three chemical mixtures. First, we calculated a set of scaled solar models ( $[\text{C}/\text{Fe}] = [\text{N}/\text{Fe}] = [\text{O}/\text{Fe}] = 0$ ). Next, we calculated a set of intermediate N-enhancement models with  $[\text{C}/\text{Fe}] = [\text{O}/\text{Fe}] = -0.1$  and  $[\text{N}/\text{Fe}] = +0.5$ . Lastly, we calculated a set of enriched N-enhancement models with  $[\text{C}/\text{Fe}] = [\text{O}/\text{Fe}] = -0.6$  and  $[\text{N}/\text{Fe}] = +1.0$ . For the enhanced models, the C

and O abundances were chosen to keep the  $[(\text{C}+\text{N}+\text{O})/\text{Fe}]$  the same between the models, according to what we observe in standard GCs (Brown, Wallerstein & Oke 1991; Cohen & Meléndez 2005; Yong, Grundahl & Norris 2015; Marino et al. 2016). For each of these chemical mixtures we kept the helium abundance (surface  $Y = 0.248$ ) constant and all other abundances fixed at solar. We assumed that the model atmospheres had the same chemical abundances at all stellar evolutionary stages.

To produce synthetic magnitudes, we integrated our model spectra over the filter transmission curves for WFC3<sup>2</sup> and ACS/WFC<sup>3</sup>. We then used the zeropoints provided on each instrument’s website to calculate Vega magnitudes. We find excellent agreement ( $< 0.01$  mag difference) between our scaled solar models and the photometry calculated by Choi et al. (2016).

We then used the synthetic magnitudes to find a suitable combination of colours for revealing the presence of chemical enhancement on the RGB of NGC 419. After trying several filters, we found out that using CUBI and CUnBI colours (see §2.3) appeared to be the most effective way to prove whether NGC 419 showed MPs. Accordingly, when comparing the expected spread in the RGB between the solar and intermediate models, as well as between the solar and enriched models, we obtained that  $\Delta(\text{CUnBI}) \simeq 2 \times \Delta(\text{CUBI})$ . This result is directly comparable with the data. We make comparisons with the observed spreads and discuss the outcomes in Section 4.

### 3.3 He Variations

We investigated possible effects of an enhanced He abundance on the RGB. Since the MIST isochrones are only available for one He abundance at a given metallicity, we used Padova isochrones (Bertelli et al. 2008) to perform our stellar atmosphere calculations. We assumed the same age and metallicity as in §3.1 and two different He abundances, one with  $Y = 0.25$  and one with an enhanced  $Y = 0.30$ . Synthetic photometry was calculated as in Section 3.2, adopting the same solar and enriched chemical mixtures.

We obtained that the difference between the standard and enhanced He models in CUBI and CUnBI colours resulted to be  $\sim 0.01$ , in the same direction for both solar and enriched mixtures. Hence, these colours are not sensitive to He variations in the RGB and we did not account for enhanced He in our analysis.

## 4 RESULTS

We compare here our model colours to the data. Figures 6 and 7 show the CUBI vs.  $m_{F438W}$  and CUnBI vs.  $m_{F438W}$  CMDs of NGC 419, respectively, with three different models superimposed. The blue, green and red curves indicate isochrones for solar, intermediate and enriched abundance variations, respectively (see §3.2). Black circles indicate the selected RGB stars in both figures.

<sup>2</sup> [http://www.stsci.edu/hst/wfc3/ins\\_performance/throughputs/Throughput\\_Tables](http://www.stsci.edu/hst/wfc3/ins_performance/throughputs/Throughput_Tables)

<sup>3</sup> <http://www.stsci.edu/hst/acs/analysis/throughputs>

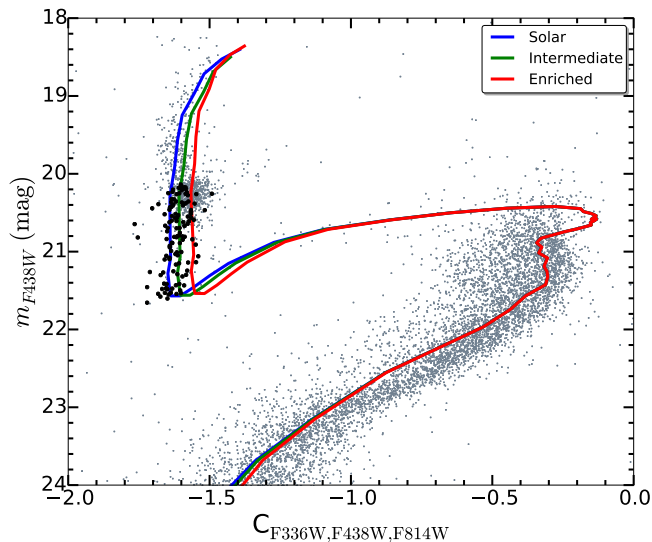


**Figure 6.**  $C_{F336W,F438W,F814W}$  vs.  $m_{F438W}$  CMD of NGC 419. Black circles indicate the selected RGB stars. The blue, green and red solid curves represent stellar evolution models ( $\log[\text{age}/\text{Gyr}] = 9.15$ ,  $[\text{Fe}/\text{H}] = -0.7$ ) for solar ( $[\text{C}/\text{Fe}] = [\text{N}/\text{Fe}] = [\text{O}/\text{Fe}] = 0$ ), intermediate ( $[\text{C}/\text{Fe}] = [\text{O}/\text{Fe}] = -0.1$ ,  $[\text{N}/\text{Fe}] = +0.5$ ) and enriched ( $[\text{C}/\text{Fe}] = [\text{O}/\text{Fe}] = -0.6$ ,  $[\text{N}/\text{Fe}] = +1.0$ ) abundance variations, respectively.

According to the models, a first look at Fig. 6 and Fig. 7 reveals that a difference in the spreads is expected if a chemical variation is present, either intermediate or enriched, between CUBI and CUnBI colours. More specifically, we calculated the average spread between the solar and the enriched models in CUBI colours and this results to be  $\simeq 0.079$ , while the average spread between these two models in CUnBI colours is  $\simeq 0.156^4$ . We then calculated the predicted spread in the RGB from the intermediate enrichment model. While the average spread in the RGB between the solar and the intermediate models in CUBI colours results to be  $\simeq 0.033$ , the average one in CUnBI colours is about  $\simeq 0.064$ . Thus, according to the models, the colour spread of stars in the RGB in CUnBI colours is expected to be twice as broad as the spread in CUBI colours, if an abundance pattern depleted in C and O and enhanced in N is present (either intermediate or enriched).

We then compared our predictions to the data. In Section 2.3, we have seen that the observed spread of RGB stars in both CUBI and CUnBI colours results in  $\sigma_{\text{data}} \sim 0.04$  ( $\sigma_{\text{CUBI}} = 0.043 \pm 0.004$  and  $\sigma_{\text{CUnBI}} = 0.043 \pm 0.003$ , see §2.3). Indeed, these spreads are consistent with that expected from the photometric errors alone. We also provided another estimation for the RGB width,  $W_{\text{RGB}}$ , and this results in  $W_{\text{RGB}} = 0.139 \pm 0.013$  for CUBI and  $W_{\text{RGB}} = 0.157 \pm 0.013$  for CUnBI, Figures 4 and 5. This proves that we do not observe any significant difference in the RGB spreads between the two colours. Hence, we do not detect the presence of multiple populations either in the form of an enriched ( $[\text{C}/\text{Fe}] = [\text{O}/\text{Fe}] = -0.6$ ,  $[\text{N}/\text{Fe}] = +1.0$ ) or intermediate ( $[\text{C}/\text{Fe}] =$

<sup>4</sup> CUBI and CUnBI spreads between the solar and enriched model and between solar and intermediate models were calculated in the RGB in a magnitude range  $20.2 \leq m_{F438W} \leq 21.2$ .

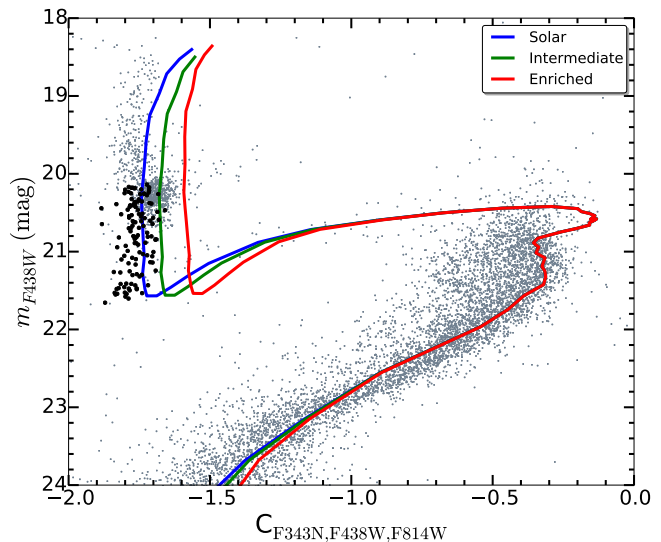


**Figure 7.** As in Fig. 6 but for  $C_{F343N,F438W,F814W}$  vs.  $m_{F438W}$  CMD.

$[\text{O}/\text{Fe}] = -0.1$ ,  $[\text{N}/\text{Fe}] = +0.5$ ) chemical anomaly in NGC 419. If MPs were present in this cluster, a detection would have been expected by simply comparing the observed width of the RGB in these two colours and by finding a significantly broader  $\sigma$  and  $W_{\text{RGB}}$  (about twice as much) in the narrow-band F343N filter colour combination. We can then conclude that no MPs are detected on the RGB of NGC 419. If MPs were present in the way they have been detected in GCs or intermediate-age clusters, we would have been able to observe them in NGC 419 as well. Our analysis can set a limit on  $[\text{N}/\text{Fe}]$  enhancement for NGC 419 to be  $< +0.5$  dex, according to what we derive from the intermediate models. However, it is crucial here to state that N enhancements previously observed in intermediate age clusters showing MPs are far higher, e.g.  $[\text{N}/\text{Fe}] > +1.0$  dex for Lindsay 1 (Hollyhead et al. 2017).

Lastly, we compared the expected spreads from the models with the observed spreads in the RC and URGB. As described in Sec. 2.3, the observed RC width in CUBI is as large as the one in CUnBI. From the models we would expect the CUBI spread to be as twice as much as the CUnBI one, if a intermediate or enriched chemical variation was present. Concerning the URGB, despite the fact that the predicted spreads in the URGB are slightly smaller than in the RGB, we still obtain a ratio between expected CUBI and CUnBI colour spreads of  $\sim 2$ . We do observe a slightly larger  $W_{\text{URGB}}$  in CUnBI than in CUBI, however they are comparable within the errors, at  $\sim 1\sigma$  confidence level ( $W_{\text{URGB}}(\text{CUBI}) = 0.105 \pm 0.012$ ,  $W_{\text{URGB}}(\text{CUnBI}) = 0.129 \pm 0.016$ ).

## 5 DISCUSSION AND CONCLUSIONS

In this paper, we analysed new and archival HST images of the SMC cluster NGC 419. We selected RGB stars by using three different CMDs and colour combinations ( $F438W - F814W$ ,  $F555W - F814W$ ,  $F336W - F438W$ ). We used the pseudo-colour indices  $C_{F336W,F438W,F814W}$  (CUBI) and  $C_{F343N,F438W,F814W}$  (CUnBI) in order to maximise the ef-

fects of multiple populations on the CMDs along the RGB. No splittings were detected, specifically in the lower RGB. Hence, we quantified the spreads in CUBI and CUnBI colours of RGB stars and compared them: these have resulted to be almost equal for both filters ( $\sigma_{\text{data}} = 0.043$ ,  $W_{\text{RGB}}(\text{CUBI}) = 0.139 \pm 0.013$ ,  $W_{\text{RGB}}(\text{CUnBI}) = 0.157 \pm 0.013$ ).

We generated MIST isochrones to have an estimate of the age and metallicity of NGC 419 and used these to develop models with different chemical anomalies. A solar, intermediate and enriched levels of enhancement have been adopted for a comparison with data. The predicted spread in CUBI between solar and enriched isochrones was found to be half as broad as the CUnBI spread. The same outcome is seen in the spreads between solar and intermediate isochrones.

We would have expected a significant variation in the observed spreads between CUBI and CUnBI colours if MPs were present in NGC 419. We can firmly conclude that no MPs are detected in the RGB of this young ( $\sim 1.4$  Gyr) and massive ( $\gtrsim 2 \times 10^5 M_{\odot}$ ) star cluster. According to our analysis, we can put a limit on [N/Fe] enhancement for NGC 419 to be  $< +0.5$  dex, which is much lower compared to spreads observed in intermediate age clusters showing the presence of MPs (e.g., [N/Fe]  $> +1.0$  dex, Lindsay 1, Hollyhead et al. 2017).

This is not the first work to find a lack of evidence for MPs in clusters younger than  $\sim 6$  Gyr. Mucciarelli et al. (2008), (2011), (2014) studied six intermediate/young age clusters (namely: NGC 1651, 1783, 1978 and 2173; NGC 1866; NGC 1806) in the LMC and found no significant abundance spreads within them, although for each cluster this result is affected by the low number statistics of stars with spectroscopically determined abundances.

However, it is worth stressing that NGC 419 is the first cluster in our HST photometric survey which does not show evidence for MPs. In Paper I we detected MPs in the SMC cluster NGC 121, while in Paper II we detected MPs in 3 additional SMC clusters, namely Lindsay 1, NGC 339, NGC 416. This has been spectroscopically corroborated by the work by Hollyhead et al. (2017), which found abundance variations in Lindsay 1, as well. Moreover, Hollyhead et al. (in prep.) has also found spectroscopic evidence for MPs in one more SMC cluster, Kron 3. All the GCs studied so far in our survey reside in the SMC and they are massive, ranging between  $\sim 1 - 2 \times 10^5 M_{\odot}$ . Nonetheless, they span a wide range in ages from 1.5 to 10 Gyr. NGC 419 is the youngest, while NGC 121 is the oldest one ( $\sim 10$  Gyr). Lindsay 1, NGC 339, NGC 416 and Kron 3 have intermediate ages (from  $\sim 6$  up to  $\sim 8$  Gyr).

Our results show that GC mass can no longer be considered as the only key physical property in order to regulate the presence of MPs (see also Cabrera-Ziri et al. 2016b). Other factors might contribute, such as age, which could play a major role in the development of MPs. Indeed, no massive GCs aged less than  $\sim 6$  Gyr have been found with chemical spreads so far. However, this would not be universal, since many less massive, Galactic open clusters older than 6 Gyr also do not host MPs (see the recent compilation by Krause et al. 2016).

We can estimate the amount of mass loss that NGC 419 will undergo over the next 4.5 Gyr (i.e. from its current age of 1.5 Gyr to an age of 6 Gyr, where clusters are ob-

served to host MPs - Hollyhead et al. 2017; Niederhofer et al. 2017a). In order to estimate this we use the rotation curve of the SMC measured by Stanimirović, Staveley-Smith & Jones (2004) and extrapolate the observations to the galactocentric distance of NGC 419, namely  $\sim 10$  kpc (Glatt et al. 2008), obtaining an estimate of 60 – 70 km/s. We also assume that the cluster is tidally filling (in order to maximise the stellar mass loss). We apply equation 7 of Kruijssen & Mieske (2009) (see also Baumgardt & Makino 2003, equation 10 and Lamers et al. 2005) to find the dissolution timescale normalisation,  $t_0$ . Applying this normalisation to the mass of NGC 419 ( $\sim 2 \times 10^5 M_{\odot}$ ) to find the dissolution timescale,  $t_{\text{dis}} = t_0 * M^{\gamma}$  (adopting  $\gamma = 0.62$  - e.g., Kruijssen & Mieske 2009), we find a  $t_{\text{dis,NGC419}} = 152$  Gyr. If we assume that the cluster loses mass linearly (see the discussion in Lamers et al. 2005) we find that over the next 4.5 Gyr the cluster will lose  $\sim 3\%$  of its mass<sup>5</sup>. Additionally, the cluster is expected to lose of order 9% of its mass due to stellar evolution. NGC 419 is expected to lose, in total, roughly  $\sim 12\%$  of its current mass over the next 4.5 Gyr (this is an upper limit as we assumed it was tidally limited). Hence, we conclude that NGC 419 (similarly to the other clusters in our sample in the SMC/LMC, with  $M \gtrsim 10^5 M_{\odot}$ ) is not expected to undergo significant mass loss over the next few Gyr (see also Cabrera-Ziri et al. 2016a).

In addition to this, in the same galaxy (i.e., the SMC), we have found both the presence and absence of the MPs phenomenon. Glatt et al. (2008) reported the distribution of star clusters in the SMC, by using distances derived from isochrones fitting. We noticed that our sample of clusters appears to be distributed over a large range of distances with respect to the galaxy centroid. NGC 339 results to be the closest to the SMC centre ( $\sim 0.7 \pm 2.0$  kpc), although with a relatively large uncertainty. This is followed by NGC 416 with a distance of  $\sim 4$  kpc, Kron 3 ( $\sim 7$  kpc) and NGC 121 ( $\sim 9$  kpc). The furthest cluster is Lindsay 1 (more than 13 kpc away), while our cluster, NGC 419, is  $\sim 10$  kpc away from the SMC centre. Accordingly, it appears that the mechanism responsible for enrichment does not depend strongly on the current environment which surrounds the cluster.

To date, the youngest GCs which show MPs are NGC 416 (Niederhofer et al. 2017a) and Kron 3 (Hollyhead et al. in prep). At this age ( $\sim 6$  Gyr) and metallicity ([Fe/H]  $\simeq -1$ ) we are sampling RGB stars with masses of  $\sim 1 M_{\odot}$ , while at the age of NGC 419 ( $\sim 1.5$  Gyr) we search for MPs at stellar masses of  $1.6 M_{\odot}$ , in the RGB. Hence, our results might also imply that the MPs phenomenon could manifest only below  $\sim 1 M_{\odot}$  and be also due to a stellar evolutionary effect. However, further investigations are needed to confirm whether this is the case.

As stated in §1, NGC 419 shows one of the largest eMSTO, well noticeable in the  $m_{F438W} - m_{814W}$  and  $m_{F555W} - m_{814W}$  vs.  $m_{814W}$  CMDs in Fig. 2 and also in CUBI and CUnBI colours (Fig. 4 and Fig. 5). Although this is beyond the scope of this paper, our results place limits on the explanation of the eMSTO feature as an age spread (Goud-

<sup>5</sup> For this, we assumed a circular orbit around the SMC for NGC 419. If we assume a high eccentricity orbit, the mass loss rate due to dissolution could be up to a factor of  $\sim 2$  higher.



frooij et al. 2014). Indeed, if multiple SF episodes due to gas processed by a first generation of stars occurred within the cluster, this would lead to self-enrichment. We did not observe any chemical spread in NGC 419, hence our data might lend support to alternative interpretations, e.g. that the MS spread is caused by a distribution of rotational velocities (e.g., Bastian & de Mink 2009; Brandt & Huang 2015; Niederhofer et al. 2015; Wu et al. 2016).

The results presented in this paper, along with Paper I & Paper II, highlight that age could play a decisive role in determining the presence of MPs. On the contrary, mass or environment can be excluded as the only key factors in this scenario. However, a larger sample is needed in order to confirm such trends. We will continue our analysis of Magellanic Cloud clusters aged  $\lesssim 1 - 2$  Gyr whose data are already in hand and present the results in forthcoming papers.

## ACKNOWLEDGMENTS

We thank Diederik Kruijssen and Henny Lamers for constructive and helpful discussions on cluster mass loss. We, in particular F.N., N.B., I.P. and V. K.-P., gratefully acknowledge financial support for this project provided by NASA through grant HST-GO-14069 for the Space Telescope Science Institute, which is operated by the Association of Universities for Research in Astronomy, Inc., under NASA contract NAS526555. N.B. gratefully acknowledges financial support from the Royal Society (University Research Fellowship) and the European Research Council (ERC-CoG-646928-Multi-Pop). We are grateful to Jay Anderson for sharing with us his ePSF software. D.G. gratefully acknowledges support from the Chilean BASAL Centro de Excelencia en Astrofísica y Tecnologías Afines (CATA) grant PFB-06/2007.

## REFERENCES

- Anderson J., King I. R., 2006, PSFs, Photometry, and Astronomy for the ACS/WFC. Tech. rep.
- Asplund M., Grevesse N., Sauval A. J., Scott P., 2009, *ARA&A*, 47, 481
- Bastian N., de Mink S. E., 2009, *MNRAS*, 398, L11
- Bastian N. et al., 2016, *MNRAS*, 460, L20
- Baumgardt H., Makino J., 2003, *MNRAS*, 340, 227
- Bertelli G., Girardi L., Marigo P., Nasi E., 2008, *A&A*, 484, 815
- Brandt T. D., Huang C. X., 2015, *ApJ*, 807, 25
- Brodie J. P., Strader J., 2006, *ARA&A*, 44, 193
- Brown J. A., Wallerstein G., Oke J. B., 1991, *AJ*, 101, 1693
- Cabrera-Ziri I. et al., 2016a, *MNRAS*, 457, 809
- Cabrera-Ziri I., Lardo C., Davies B., Bastian N., Beccari G., Larsen S. S., Hernandez S., 2016b, *MNRAS*, 460, 1869
- Carretta E., Bragaglia A., Gratton R. G., D’Orazi V., Lucatello S., Sollima A., 2014, *A&A*, 561, A87
- Choi J., Dotter A., Conroy C., Cantiello M., Paxton B., Johnson B. D., 2016, *ApJ*, 823, 102
- Cohen J. G., Meléndez J., 2005, *AJ*, 129, 303
- Colucci J. E., Bernstein R. A., Cameron S. A., McWilliam A., 2012, *ApJ*, 746, 29
- Dalessandro E., Lapenna E., Mucciarelli A., Origlia L., Ferraro F. R., Lanzoni B., 2016, *ApJ*, 829, 77
- Dotter A., 2016, *ApJS*, 222, 8
- Glatt K. et al., 2008, *AJ*, 136, 1703
- Goudfrooij P. et al., 2014, *ApJ*, 797, 35
- Goudfrooij P., Puzia T. H., Kozhurina-Platais V., Chandar R., 2009, *AJ*, 137, 4988
- Gratton R., Carretta E., Bragaglia A., 2012, *A&ARv*, 20, 50
- Hartigan J. A., Hartigan P. M., 1985, *The Annals of Statistics*, 13, 70
- Hollyhead K. et al., 2017, *MNRAS*, 465, L39
- Krause M. G. H., Charbonnel C., Bastian N., Diehl R., 2016, *A&A*, 587, A53
- Kruijssen J. M. D., Mieske S., 2009, *A&A*, 500, 785
- Kurucz R. L., 1970, *SAO Special Report*, 309
- Kurucz R. L., 2005, *Memorie della Societa Astronomica Italiana Supplementi*, 8, 14
- Kurucz R. L., Avrett E. H., 1981, *SAO Special Report*, 391
- Kurucz R. L., Furenlid I., 1979, *SAO Special Report*, 387
- Lamers H. J. G. L. M., Gieles M., Bastian N., Baumgardt H., Kharchenko N. V., Portegies Zwart S., 2005, *A&A*, 441, 117
- Larsen S. S., Brodie J. P., Forbes D. A., Strader J., 2014a, *A&A*, 565, A98
- Larsen S. S., Brodie J. P., Grundahl F., Strader J., 2014b, *ApJ*, 797, 15
- Larsen S. S., Brodie J. P., Strader J., 2012, *A&A*, 546, A53
- Mackey A. D., Broby Nielsen P., Ferguson A. M. N., Richardson J. C., 2008, *ApJL*, 681, L17
- Marino A. F. et al., 2016, *MNRAS*, 459, 610
- Milone A. et al., 2012, *A&A*, 540, A16
- Milone A. P., Bedin L. R., Piotto G., Anderson J., 2009, *A&A*, 497, 755
- Milone A. P. et al., 2015, *MNRAS*, 450, 3750
- Monelli M. et al., 2013, *MNRAS*, 431, 2126
- Mucciarelli A., Carretta E., Origlia L., Ferraro F. R., 2008, *AJ*, 136, 375
- Mucciarelli A. et al., 2011, *MNRAS*, 413, 837
- Mucciarelli A., Dalessandro E., Ferraro F. R., Origlia L., Lanzoni B., 2014, *ApJ*, 793, L6
- Mucciarelli A., Origlia L., Ferraro F. R., Pancino E., 2009, *ApJ*, 695, L134
- Niederhofer F. et al., 2017a, *MNRAS*, 465, 4159
- Niederhofer F. et al., 2017b, *MNRAS*, 464, 94
- Niederhofer F., Georgy C., Bastian N., Ekström S., 2015, *MNRAS*, 453, 2070
- Piotto G. et al., 2015, *AJ*, 149, 91
- Rubele S., Kerber L., Girardi L., 2010, *MNRAS*, 403, 1156
- Salinas R., Strader J., 2015, *ApJ*, 809, 169
- Sbordone L., Bonifacio P., Castelli F., Kurucz R. L., 2004, *Memorie della Societa Astronomica Italiana Supplementi*, 5, 93
- Sbordone L., Salaris M., Weiss A., Cassisi S., 2011, *A&A*, 534, A9
- Stanimirović S., Staveley-Smith L., Jones P. A., 2004, *ApJ*, 604, 176
- Villanova S., Geisler D., Carraro G., Moni Bidin C., Muñoz C., 2013, *ApJ*, 778, 186
- Wu X., Li C., de Grijs R., Deng L., 2016, *ApJL*, 826, L14
- Yong D., Grundahl F., Norris J. E., 2015, *MNRAS*, 446, 3319